Draft version April 12, 2021
Typeset using LaTeX **modern** style in AASTeX63

Revisit the Oort constants from *Gaia DR2* observations and simulations

Shufan Xia,[1] Karens Masters,[1] and Zhao-Yu Li[2]

[1]*Haverford College, Department of Physics and Astronomy*
[2]*Shanghai Jiaotong University, Department of Astronomy*

1. INTRODUCTION

2. METHODS

$$v_{los} = d[K + A\sin(2l) + C\cos(2l)] - u_0\cos(l) - v_0\sin(l) \tag{1}$$

$$\mu_l = B + A\cos(2l) - C\sin(2l) + \frac{1}{d}[u_0\sin(l) - v_0\cos(l)] \tag{2}$$

$$\mu_b = -(Asin2l + Ccos2l + K)sinb\,cosb + \varpi[(u_0cosl + v_0sinl)sinb - w_0cosb] \tag{3}$$

3. RESULTS

This paper uses the following notation for velocity components: In Galactocentric coordinate: v_{circ} or v_ϕ is the circular velocity about the Galactic Center(GC), v_r is the radial velocity with respect to the GC and v_z is vertical velocity away from the Miky Way (MW) disk. In Galactic coordinate: v_{los} is the line of sight velocity as seen from the Sun, v_l is the velocity component perpendicular to the line of sight in the l direction, and v_b represents the velocity component perpendicular to the line of sight in the b direction.

For our simulation, because we set the peculiar motion of the Sun to 0, the coordinate and velocity of LSR and the Sun are equivalent.

3.1. *Simulation: The effect of sampling criteria on μ_l, v_{los}, μ_b*

With 500000 simulated stars (test particles), we examined the effect of different sampling criteria on the resulting proper motions (μ_l and μ_b) and the line-of-sight velocity (v_{los}) dependency on l. Fig 1a displays the distribution of the 500,0000

Corresponding author: Shufan Xia
sxia1@haverford.edu

samples, and Fig 1b shows those within $d = 4$ kpc from the Sun and how I replicated the Sun's position to increase the number of stars in this range for the purpose of analyzing the simulation results.

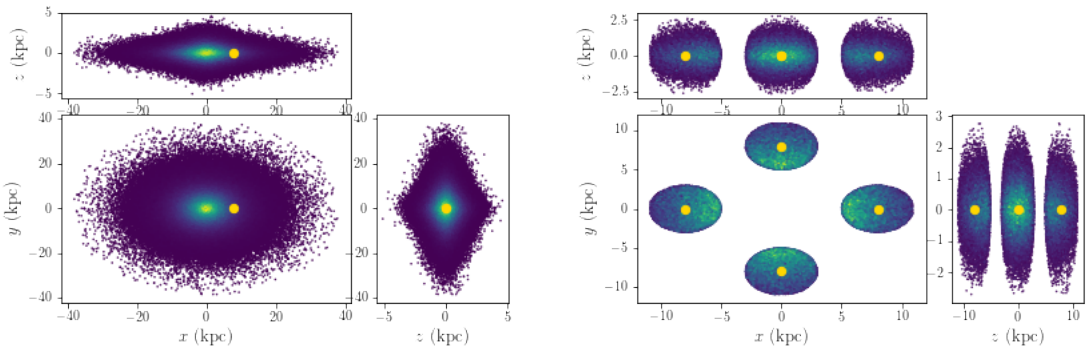

(a) (b)

Figure 1: (a)The distribution of the 500,0000 test particles (stars) sampled from quasi-isothermal distribution function for the Milky Way. (b) The distribution of simulated stars withi $d = 4$kpc from the Sun, where I replicated the Sun at four different positions to increase effective samples near the Sun.

3.1.1. μ_l *and* v_{los}

Fig 2 shows the result of μ_l vs l function under three sample filtering criteria on the galactic distance d for stars at $|b| < 20°$. Proper motions after correcting the contribution in latitudinal direction ($\cos b$) are mostly negative across $l = 0°$ to $360°$, indicating that stars move in the decreasing l direction. Fig 2 also shows μ_l has close to 0 but positive value at $l = 0°, 180°$, and $360°$. μ_l is most negative and has larger variation among stars with the same l value at $l = 90°$ and $270°$, as compared to the stars at $l = 0°, 180°$, or $360°$.

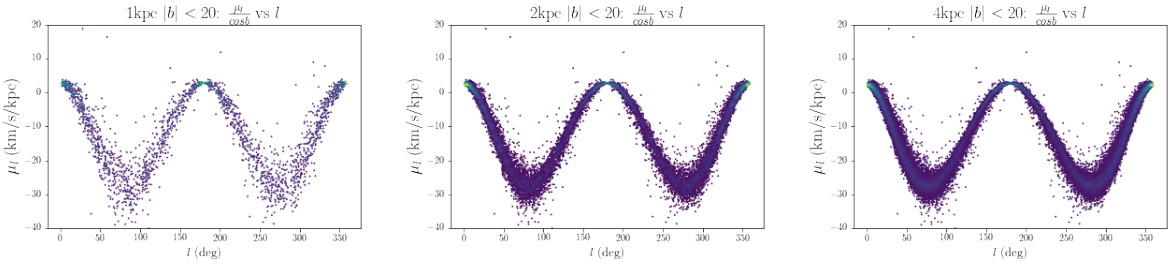

(a) (b) (c)

Figure 2: The distribution of $\mu_l / \cos b$ over l for stars with $|b| \leq 20$ and ,(a) $d \leq$ 1kpc,(b) $d \leq$ 2kpc, and (c) $d \leq$ 4kpc

The function of v_{los} vs l for stars with $d <$ 2kpc and $|b| < 20$ is in Fig 3a. The data color-coded by d value suggests for each similar d value, the v_{los} vs l function follows

a distinct double sine curve. The larger d is, the amplitude of the v_{los} vs l function is larger. Fig 15d shows v_{los} after divided by d traces a single double sinusoidal function as expected from Eq1. v_{los} is 0 at $l = 0°, 90°, 180°, 270°$. Positive v_{los} between $l = 0°$ to 90° and $l = 180°$ and 270° suggests stars approach the Sun, while they move away from the Sun in the line of sight direction between $l = 90°$ and $180°, 270°$ and 360°. In Fig 3, I further compared v_{los}/d vs l function under three sample filtering criteria on d while keeping $|b| < 20°$ in Fig3b and 3d.

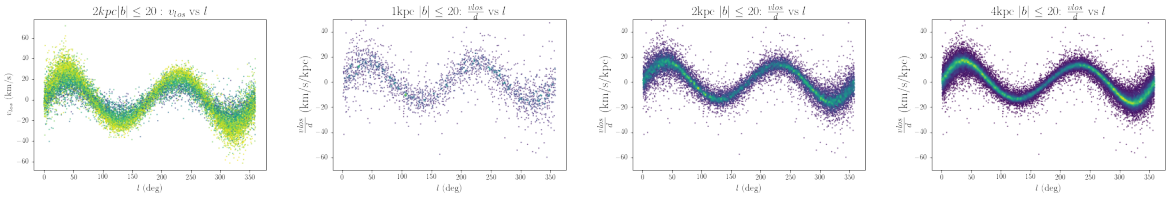

(a) (b) (c) (d)

Figure 3: (a) The distribution of v_{los} over l for stars with $|b| \leq 20$ and $d < 2$kpc. The distribution of v_{los}/d over l for stars with $|b| \leq 20$ and (b) $d \leq 1$kpc,(d) $d \leq 2$kpc, and (d) $d \leq 4$kpc

Fig4 gives a simplified vector analysis on the velocities of stars nearby the Sun at different while ignoring vertical distributions and motions. Assume these stars are in all circular orbits with radius R_{star}s, and when R_{star} is close to $R_{\odot}$, v_{ϕ}s are approximately in the same direction). At $l = 0°$ and 180°, v_{ϕ}s of stars and LSR are in the same direction, and v_{ϕ} is perpendicular to the line of sight. As a result, $v_{los} = 0°$ and $v_l = v_{\phi} - v_{\phi\odot}$ of the sun. According to the rotation velocity curve in (introduction figure), v_{ϕ} is flat while slightly declining at $R = R_{\odot}$. As a result, thus μ_l has a small positive at $l = 0°$ which is in the inner side of the MW disk compared to the Sun. And at l=180, (because xxx,) this v_{ϕ} difference is also positive. At $l = 90°$ and 270°, stars are approximately in the same circular orbits as the Sun. They are essentially moving at the same speed as the sun along the line of sight, thus $v_{los} = 0°$. v_l has the most negative value (because xxx). At $l = 45°$ and 225°, the outward-pointing velocity component in the line-of-sight direction shows the stars are moving in the direction of the Sun away from the Sun. And at $l = 135°$ and 315°, ... (I need to discuss this with my thesis advisor).

3.1.2. *The effect of d on μ_l and v_{los}*

The number of samples selected drops from 51196 to 16741 and to 2310 as the distance cut-off decreases from 4kpc, to 2kpc, and to 1kpc in Fig2 and Fig3. The spreads of μl and v_{los} are unaffected by the d cut-off chosen.

However, the binned median values reveal some differences. Fig5 shows the medians of μ_l after grouping all scatter data in Fig2 into bins with a width of $l = 5°$. The error bars in Fig5 are the standard deviations of the corresponding bins. For the simulated

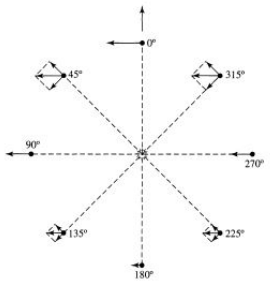

Figure 4: The variation in the radial velocity and transverse velocity among different Galactic longitude due to differential rotation of the Milky Way (Carroll & Ostlie 2007)

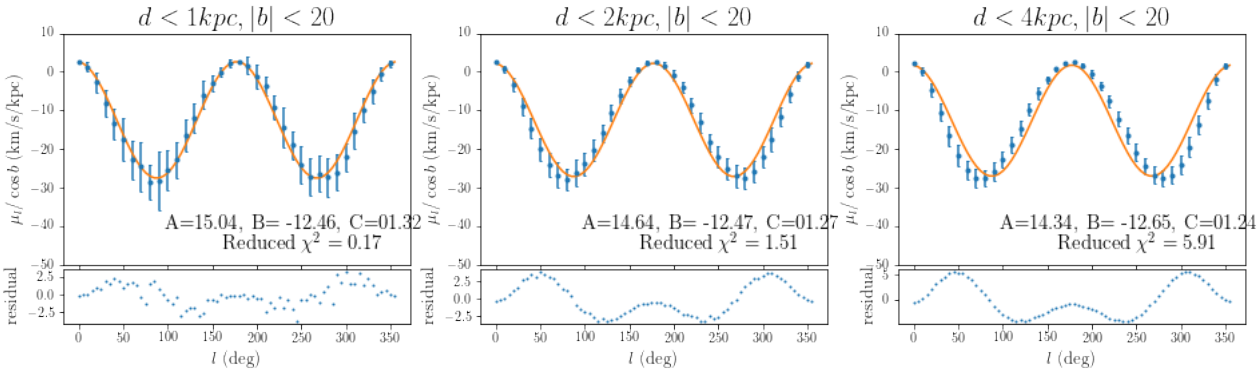

(a) (b) (c)

Figure 5: The function of binned median $\mu_l/\cos b$ over l for stars with $|b| \leq 20°$ and ,(a) $d \leq$ 1kpc,(b) $d \leq$ 2kpc, and (c) $d \leq$ 4kpc.The orange continuous curves come from fitting the binned median data to Eq2 with maximum likelihood approximation. Only 36 out of 72 binned medians are plotted.

stars within 4kpc, there are significant deviations from the double cosine function, implying 4kpc is too large for the Taylor approximation in Oort constant derivation. The stars within 2kpc yield a reduced χ^2 that is closest to 1. However, including higher-order and terms, such as $\sin(3l)$, $\cos(3l)$, etc would fit these simulated data points more accurately. The proper motions of stars within 1kpc from the sun trace the double sinusoidal function best compared to 2kpc and 4kpc, and the residuals are also smallest for this group. However, this sampling choice only yielded 2310 out of 500,000 that meet this filtering criteria, and this smaller sample size results in a larger standard deviation within each bin as the spread of scattered data around the median stay the same in Fig2(Wrong. Needs to revise here).

Similarly, the binned v_{los} median of stars within $d <$ 1kpc and $|b| < 20°$ give v_{los}/d vs l function closet to the function in Eq1 compared to stars within 4kpc and 2kpc (Fig6).

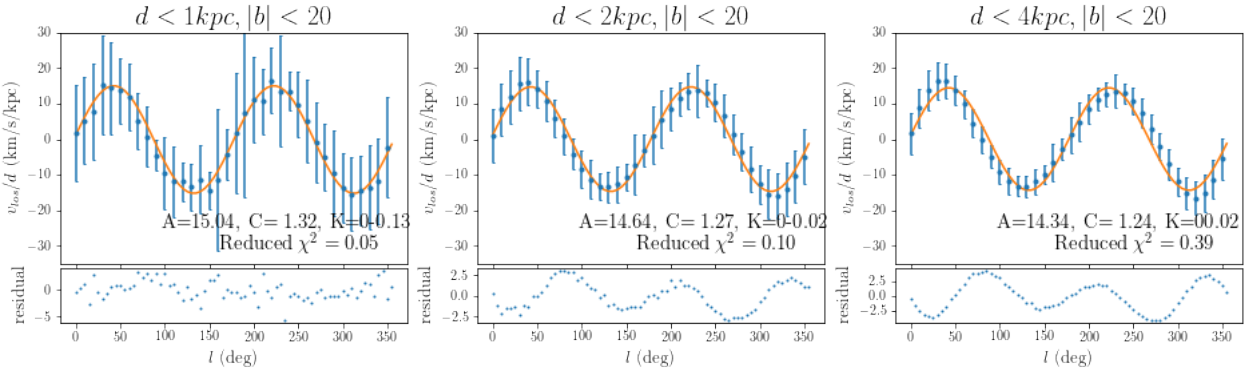

(a) (b) (c)

Figure 6: The function of binned median v_{los}/d over l for stars with $|b| \leq 20°$ and ,(a) $d \leq$ 1kpc,(b) $d \leq$ 2kpc, and (c) $d \leq$ 4kpc.The orange continuous curves come from fitting the binned median data to Eq1 with maximum likelihood approximation. Only 36 out of 72 binned medians are plotted.

comment on reduced χ^2: Not a very helpful number to look at, residual vs l plot is better.

3.1.3. *The effect of b on μ_l and v_{los}*

Comparing stars with $d <$ 2kpc but at different latitude ranges in Fig7 shows the scatter in the μ_l around the central double sinusoidal line increases for higher latitude regions. With a larger b value, we move further away from the Milky Way (MW) disk, and the orbits there get less circular because MW potential gradient in the z-direction is large enough to add significant vertical perturbations, tilting the circular orbits that would otherwise stay on a plane parallel to the MW mid-plane (consult Galactic Dynamics Merrifield). In Fig 8, binned μ_l median vs l is compared for the four filtering criteria on b range. The difference between $|b| \leq 10°$ and $|b| \leq 20°$ is hard to tell based on Chi-square and residuals, but the number of samples with $|b| \leq 20°$ is about twice as many as $|b| \leq 10°$. For $30° \leq |b| \leq 50°$, the scattered data deviate from the double cosine function considerably. And for $60° \leq |b| \leq 80°$, not only the spread in the scattered data is the largest, the binned medians deviate from the fitted double cosine function more significantly as evidenced by the residual vs l panel below in Fig **??**.

Similarly, the spread in the v_{los}/d of simulated stars with $d <$ 2kpc at higher latitude b is larger in Fig**??**. And the deviation of binned v_{los}/d median from the predicted double sin function is largest for stars at 60¡—b—¡80 (Fig**??**).

Based on the discussion above, I chose $d <$ 2kpc and —b—¡20 as the sampling criteria for analyzing μ_l and v_{los}. With MCMC, I determined the best-fitting parameters and their uncertainty: $A = 14.84 \pm e1, B == 12.47 \pm e2, C = 1.27 \pm e3, K = 0.02 \pm e4$, in the unit of km/s/kpc.

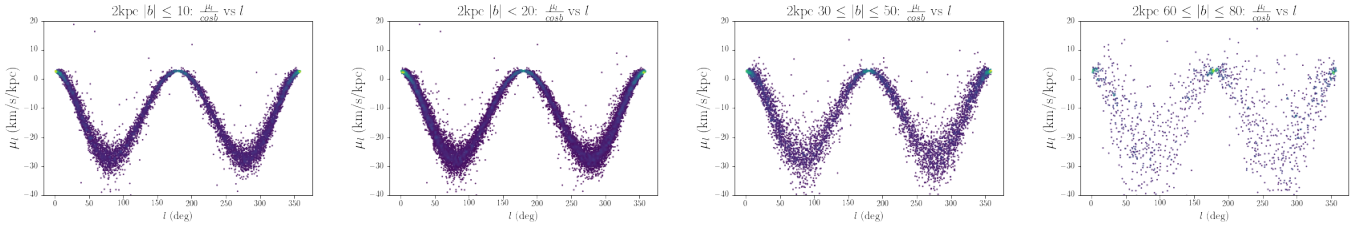

(a) (b) (c) (d)

Figure 7: The distribution of $\mu_l/\cos b$ over l for stars with $d < 2$kpc and (a) $|b| < 10°$, (a) $|b| < 20°$, (c) $30° \leq |b| \leq 50°$, and (d) $60| < 80°$.

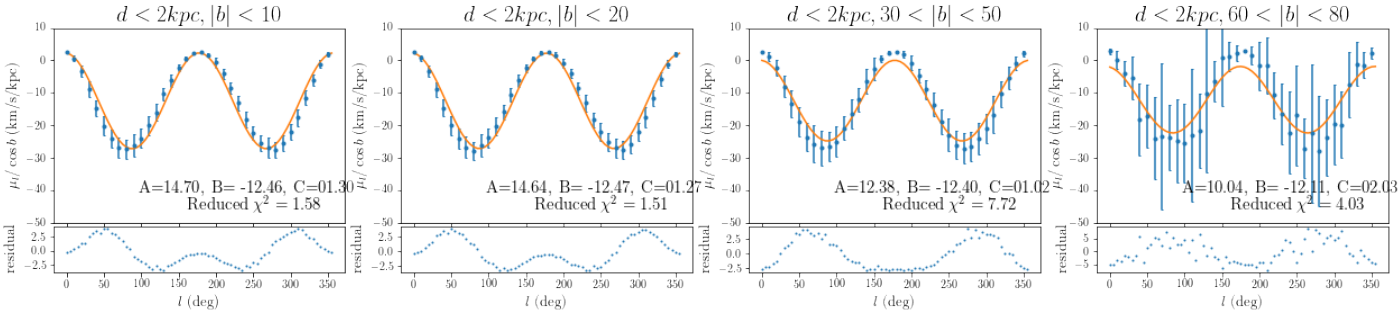

(a) (b) (c) (d)

Figure 8: The function of binned median $\mu_l/\cos b$ over l for stars with $d < 2$kpc and (a) $|b| \leq 10°$, (b) $|b| \leq 20°$,(c) $30°|b| \leq 50°$, and (d) $60°|b| \leq 80°$.

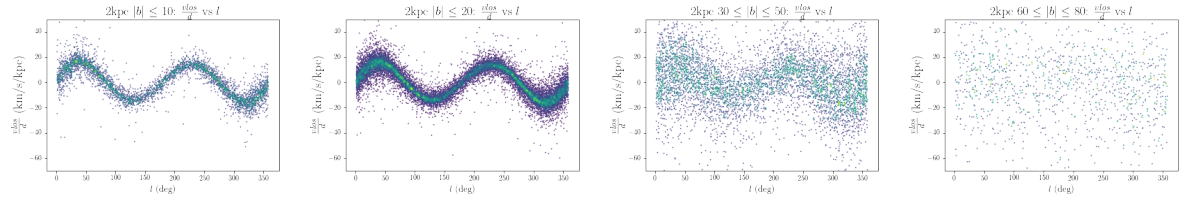

(a) (b) (c) (d)

Figure 9: The distribution of v_{los}/d over l for stars with $d < 2$kpc and (a) $|b| < 10°$, (d) $|b| < 20°$, (c) $30° \leq |b| \leq 50°$, and (d) $60| < 80°$.

3.1.4. μ_b

For proper motion in the latitude direction, μ_b, we expected to see more nonzero value at the middle $|b|$ region because of the product $\sin b \cos b$ in Eq3. Different from μ_b and v_{los} in Fig2 and 9, the scatter data points of $\mu_b/\cos b \sin b$ of stars with $d < 2$kpc, $30 < |b| < 50$ in Fig11 are much more dispersed. In Fig 12, taking binned medians gives the expected double sinusoidal curve. The binned standard deviations for these binned μ_b medians range from 50-100 km/s/kpc, much larger than the variation of the binned medians across l, ($\pm$25km/s/kpc). Thus, error bars are not

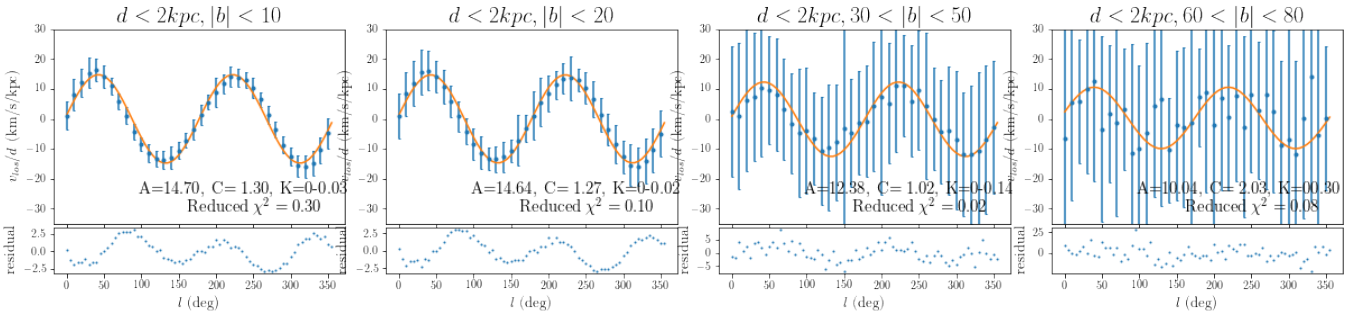

(a) (b) (c) (d)

Figure 10: The function of binned median v_{los}/d over l for stars with $d < 2$kpc and (a) $|b| \leq 10°$, (b) $|b| \leq 20°$,(c) $30°|b| \leq 50°$, and (d) $60°|b| \leq 80°$.

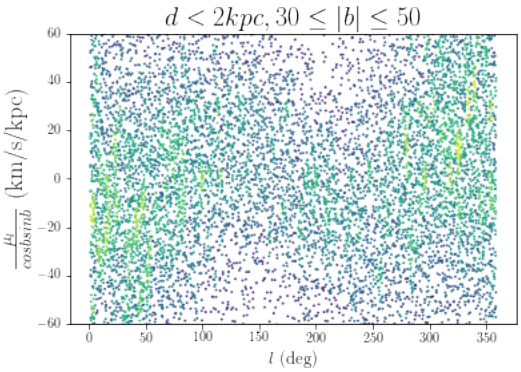

Figure 11: $\mu_b/\cos b \sin b$ of stars with $d < 2$kpc, $30° < |b| < 50°$

plotted in Fig12 to better show the dependency of binned $\mu_b/\cos b \sin b$ medians on l. At $l = 0°, 90°, 180°, 270°$, $\mu_b = 0$. Stars are descending from the perspective of LSR for $l = 0 \sim 90°$ and $180 \sim 270°$ while ascending for $l = 90 \sim 180°$ and $270 \sim 360°$.

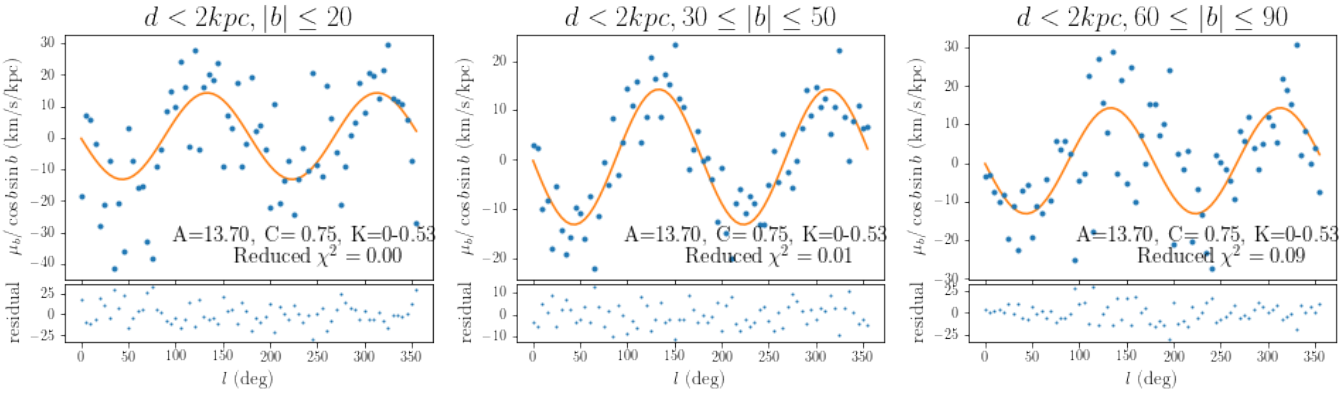

(a) (b) (c)

Figure 12: The function of binned median $\mu_b/\cos b \sin b$ over l for stars with $d < 2$kpc and ,(b) $|b| \leq 20°$,(b) $30°|b| \leq 50°$, and (c) $60°|b| \leq 90°$

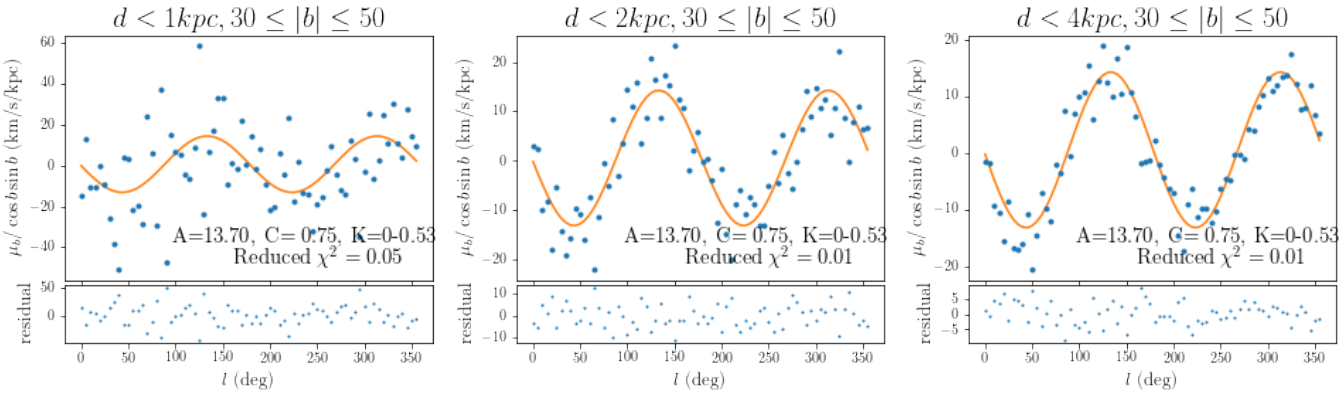

(a) (b) (c)

Figure 13: The function of binned median $\mu_b/\cos b \sin b$ over l for stars with $30°|b| \leq 50°$ and ,(a) $d \leq 1$kpc,(b) $d \leq 2$kpc, and (c) $d \leq 4$kpc.

While the derivation of Oort constants assumes stars are close to the MW mid-plane and, thus, the discussion on μ_l and v_{los} is more prevalent in textbooks (cite), proper motion in the latitudinal direction is also a kinematic tracer of the MW differential rotation. Assume we have a star at some vertical distance from the MW mid-plane and on a circular orbit with a constant v_ϕ and v_z= 0, because of the MW differential rotation this v_ϕ is different and moves toward the Sun as l varies. The change in the title angle of the line-of-sight at different l will result in a change in μ_b (Fig14). This component is larger for stars with higher b because of the $\sin b$ component. Therefore, μ_b is also an indicator of the in-plane motion. However, for stars with very high b, that is away from the disc in the vertical direction, their orbits are rather non-circular due to the potential perturbation in the vertical direction. These stars tend to have larger vertical velocities, which potentially give a more dominant contribution to μ_b than differential rotation. As shown In Fig12, compared to the stars closer to the MW disk ($|b| < 20°$) or those that are much farther away from the MW disk ($|b| > 60°$), stars with $|b|$ between 30° and 50° yield the most noticeable double sin variation with l.

On the other hand, in Fig13, for larger spatial coverage, $d < 4$kpc, binned median of $\mu_b/\cos b \sin b$ follows the double sine function better than stars within 2kpc and 1kpc, which is also suggested by the residual vs l panels. (Why? Need more investigations: 1)increase in sample size, 2)...)

3.2. *The effect of radial and vertical velocity profiles on μ_l, v_{los}, μ_b*

Fig15 includes $\mu_l/\cos b$, v_{los}/d and binned median of μ_b as a function of l under three different velocity profiles: 1) v_r and v_z 2) $v_r = 0$ and 3) $v_z = 0$. The result shows the spread in μ_l is due to the variation of v_r. Both v_r and v_z have contributions to the scattering in v_{los}/d. When v_r is set to 0, the scattering around the central double sine curve is smaller as the brighter color indicates a higher density. Meanwhile, the

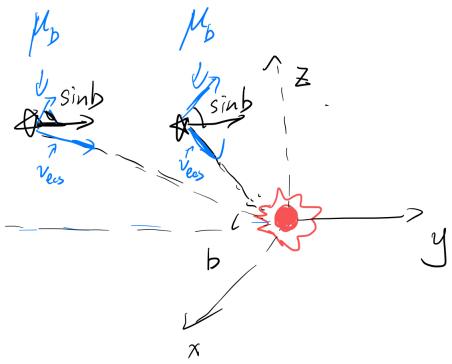

Figure 14: The change in v_b at different l

contribution to the scattering in v_{los}/d by v_z is more significant. The difference of the binned median of μ_b under three velocity profiles shows the deviations from the double sine function described by the Oort constants is attributed to the non-zero vertical velocity stars, agreeing with the discussion in section 3.1.4.

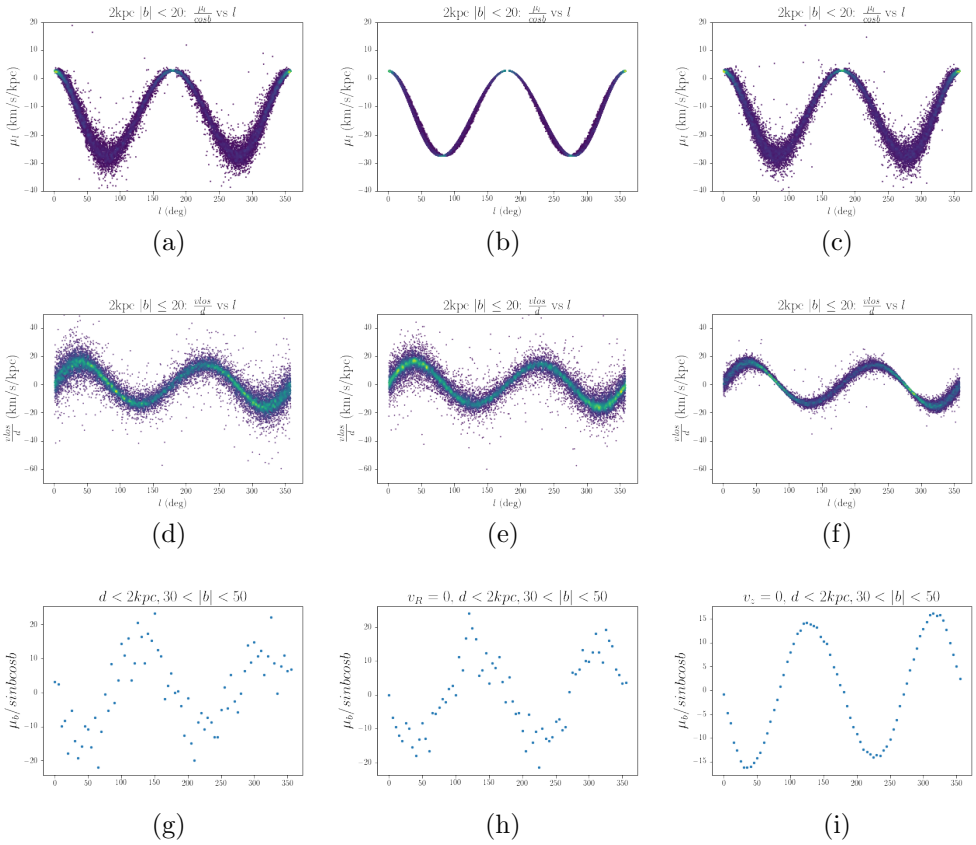

Figure 15: $\mu_l/\cos b$, v_{los}/d and binned median of μ_b as a function of l under three different velocity profiles from the leftmost to the rightmost columns: 1) v_r and v_z 2) $v_r = 0$ and 3) $v_z = 0$.

3.3. *Gaia DR2 observational data*

3.3.1. *Gaia DR2: using the filtering criteria from literature*

Fig 16 shows $\Delta\mu_l$ as a function of l for stars with $d < 500$pc and $|b| < 20°$ for stellar populations with $G_{BP} - G_{RP} - E(BP\_RP) < 0.8$, $0.8 \sim 1,2$, $1.2 \sim 1.6$, $1.6 \sim 2.0$, $2.0 \sim 2.4$ and ≥ 2.4. The plots are not quite correct. In general 1) $\Delta_{\mu l}$ fits Eq2, so we can calculate the Oort constants from this result. 2) There is a population of stars concentrated at $l = 280°$ and μ_l around 20 km/s/kpc. 3) The deviation from the double cosine function is lager for redder stellar populations as we move across panel (a) to (d) in Fig16. This is consistent with the fact that redder stars are kinematic ally older and reside in hotter thus less circular orbits.

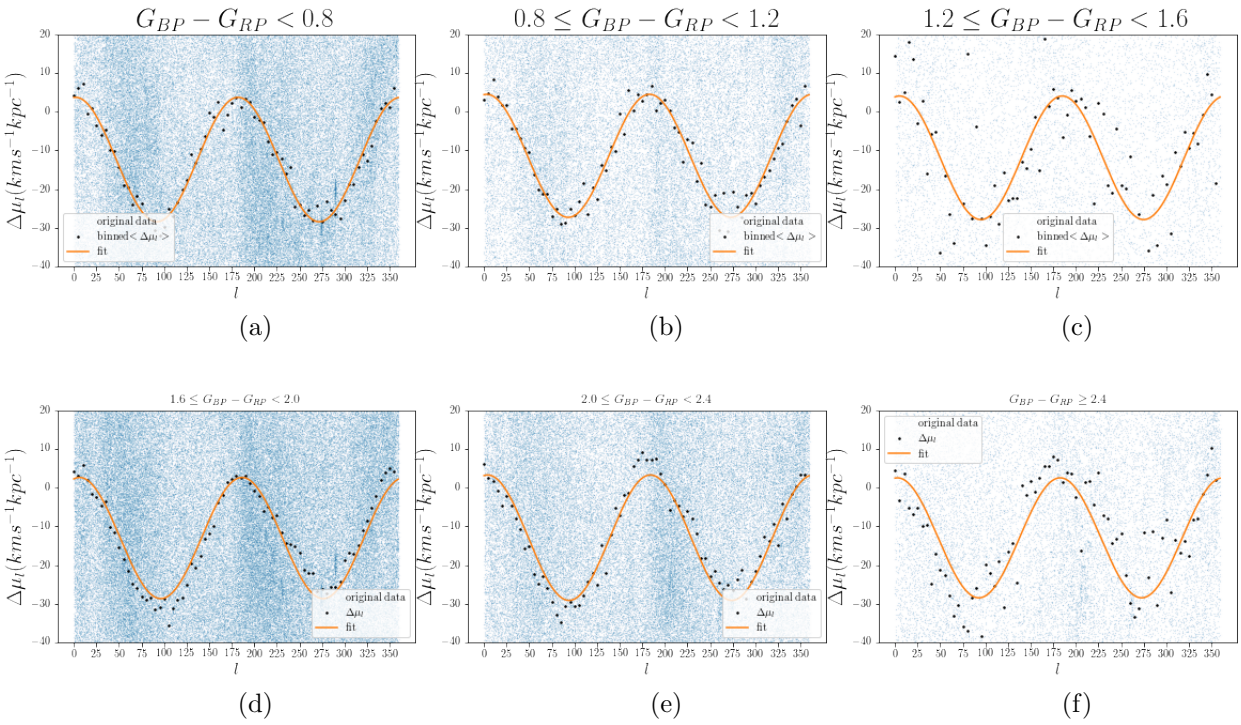

Figure 16: $\Delta\mu_l$ as a function of l for stars with $d < 500$pc and $|b| < 20°$ divided into groups with $G_{BP} - G_{RP} - E(BP\_RP) < 0.8$, $0.8 \sim 1,2$, $1.2 \sim 1,6$, $1.6 \sim 2.0$, $2.0 \sim 2.4$ and ≥ 2.4.

Similar to μ_l, v_{los}s for the two bluest stellar population calculated from the radial velocity data in DR2 are also well described by the double sine function predicted by the Oort constants (Fig17). Despite radial velocity data entry is not available for all the stars in DR2, the two bluest stellar populations in Fig17 show v_{los} can be used to derive the Oort constants. Table1 shows the estimated peculiar motion (u_0, v_0, w_0) from fitting μ_l and Fig16 by maximum likelihood estimation, and v_{los} in Fig17 is included into the log likelihood function for the three bluest stellar populations.

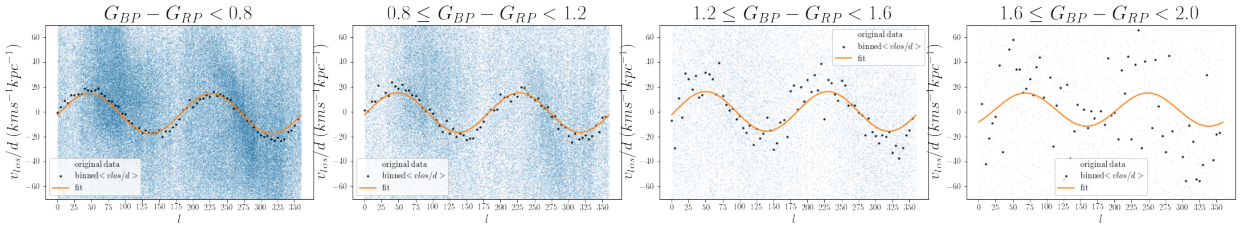

(a) (b) (c) (d)

Figure 17: Δv_{los} as a function of l for stars with $d < 500$pc and $|b| < 20°$ divided into groups with $G_{BP} - G_{RP} - E(BP\_RP) < 0.8$, $0.8 \sim 1, 2$, $1.2 \sim 1.6$, and $1.6 \sim 2.0$.

	$u_0(kms^{-1})$	$v_0(kms^{-1})$	$w_0(kms^{-1})$
$G_{BP} - G_{RP} - E(BP - RP) < 0.8$	9.98	20.30	7.51
$0.8 \leq G_{BP} - G_{RP} - E(BP - RP) < 1.2$	10.26	24.20	8.32
$1.2 \leq G_{BP} - G_{RP} - E(BP - RP) < 1.6$	10.07	25.14	7.92
$1.6 \leq G_{BP} - G_{RP} - E(BP - RP) < 2.0$	10.24	26.91	7.92
$2.0 \leq G_{BP} - G_{RP} - E(BP - RP) < 2.4$	8.76	23.91	8.00
$G_{BP} - G_{RP} - E(BP - RP) \geq 2.4$	10.41	22.72	6.71

Table 1: The value of solar peculiar motion (u_0, v_0, w_0) from fitting μ_l and v_{los} in Fig16 and Fig17 if available. (These are not correct, just for placeholder)

While the l dependencies of μ_l and v_{los} for the stars in DR2 are consistent with the equations of the Oort constants, μ_bs for stars near the Sun and with middle $|b|$ range do not follow the curve predicted by Eq3 as nicely as μ_l and v_{los} do. Only for the bluest stellar population, $\delta_{\mu b}$ follows the double sine function with deviation ± 5 (I eyeballed it, will calculate it later).

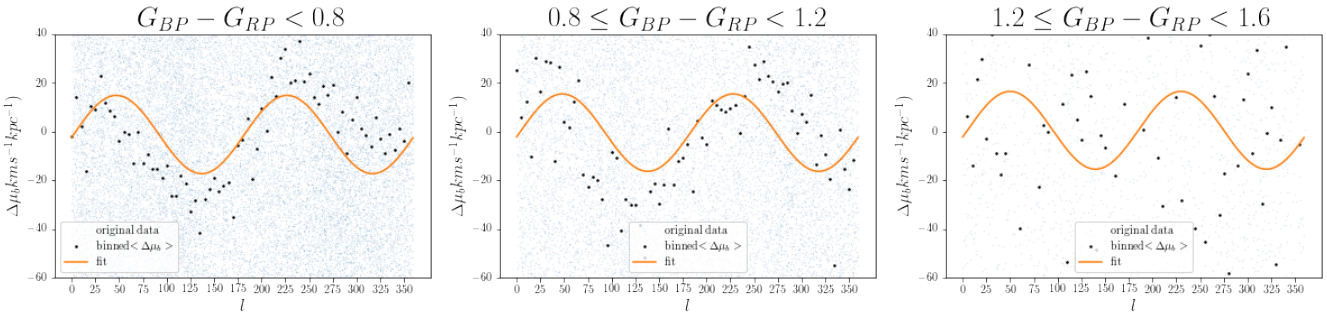

(a) (b) (c)

Figure 18: $\Delta\mu_b$ as a function of l for stars with $d < 500$pc and $40° < |b| < 50°$ divided into groups with $G_{BP} - G_{RP} - E(BP\_RP) < 0.8$, $0.8 \sim 1, 2$, and $1.2 \sim 1.6$.

Table2 lists the values of the Oort Constants and their uncertainties estimated from the results in Fig16, 17 and 18 using MCMC.

	$A(km/s/kpc)$	$B(km/s/kpc)$	$C(km/s/kpc)$	$K(km/s/kpc)$
$G_{BP} - G_{RP} - E(BP - RP) < 0.8$				
$0.8 \leq G_{BP} - G_{RP} - E(BP - RP) < 1.2$				
$1.2 \leq G_{BP} - G_{RP} - E(BP - RP) < 1.6$				
$1.6 \leq G_{BP} - G_{RP} - E(BP - RP) < 2.0$				
$2.0 \leq G_{BP} - G_{RP} - E(BP - RP) < 2.4$				
$G_{BP} - G_{RP} - E(BP - RP) \geq 2.4$				

Table 2: The values of the Oort Constants and their uncertainties estimated from the results in Fig16, 17 and 18 using MCMC.

3.3.2. *Applying filtering criteria based on Simulation to Gaia DR2*

No result yet.

REFERENCES

Carroll, B. W., & Ostlie, D. A. 2007, An Introduction to Modern Astrophysics, 2nd edn., ed. S. F. P. Addison-Wesley